

# Site-specific inhibition of the thalamic reticular nucleus induces distinct modulations in sleep architecture

Vladimir Visocky<sup>1</sup> | Brian J. Morris<sup>2</sup> | John Dunlop<sup>3</sup> | Nick Brandon<sup>3</sup> | Shuzo Sakata<sup>1</sup> | Judith A. Pratt<sup>1</sup>

<sup>1</sup>Strathclyde Institute of Pharmacy and Biomedical Sciences, University of Strathclyde, Glasgow, UK

<sup>2</sup>College of Medical, Veterinary and Life Sciences, Institute of Neuroscience and Psychology, University of Glasgow, Glasgow, UK

<sup>3</sup>AstraZeneca, Boston, Massachusetts, USA

## Correspondence

Vladimir Visocky and Judith A. Pratt, University of Strathclyde, Strathclyde Institute of Pharmacy and Biomedical Sciences, Glasgow, UK.

Email: [vladimir.visockis@nih.gov](mailto:vladimir.visockis@nih.gov) and [j.a.pratt@strath.ac.uk](mailto:j.a.pratt@strath.ac.uk)

Edited by: Antoine Adamantidis

## Abstract

The thalamic reticular nucleus (TRN) is crucial for the modulation of sleep-related oscillations. The caudal and rostral subpopulations of the TRN exert diverse activities, which arise from their interconnectivity with all thalamic nuclei, as well as other brain regions. Despite the recent characterization of the functional and genetic heterogeneity of the TRN, the implications of this heterogeneity for sleep regulation have not been assessed. Here, using a combination of optogenetics and electrophysiology in C57BL/6 mice, we demonstrate that caudal and rostral TRN modulations are associated with changes in cortical alpha and delta oscillations and have distinct effects on sleep stability. Tonic silencing of the rostral TRN elongates sleep episodes, while tonic silencing of the caudal TRN fragments sleep. Overall, we show evidence of distinct roles exerted by the rostral and caudal TRN in sleep regulation and oscillatory activity.

## KEYWORDS

EEG, optogenetics, sleep, thalamic reticular nucleus

## 1 | INTRODUCTION

Sleep is a homeostatic function preserved across the animal kingdom. The main neurobiological drivers of global sleep and arousal are found in primordial brain areas (Batini et al., 1958; Mcginty & Serman, 1968; von Economo, 1930); however, the forebrain has been found also to impact sleep quality and quantity (Siclari & Tononi, 2017). During non-rapid-eye-movement (NREM) sleep, the interplay between the thalamus and the cortex

generates major sleep rhythms: delta (1–4 Hz) and short, recurrent alpha oscillations known as sleep spindles (9–16 Hz) (Steriade et al., 1993). An atypical thalamic nucleus, the thalamic reticular nucleus (TRN), modulates sleep-related oscillations and sleep architecture via inhibitory control over other thalamic nuclei (Fernandez et al., 2018; Halassa et al., 2014, 2011; Lewis et al., 2015). For example, the rise in the sleep spindle density caused by various genetic or optogenetic manipulations on the TRN leads to prolonged or less fragmented NREM sleep (Kim et al., 2012; Ni et al., 2016; Wimmer et al., 2012) whereas the reduction in the sleep spindle density results in fragmented sleep (Li et al., 2020; Wells et al., 2016). Sleep spindles act as a hallmark of brain state change (Vyazovskiy et al., 2004). They manifest at the beginning and at end of NREM sleep (Astori et al., 2011;

**Abbreviations:** Arch, archaerhodopsin; EEG, electroencephalogram; EMG, electromyography; eYFP, green/yellow fluorescent protein; NpHR, halorhodopsin; NREM, non-rapid eye movement sleep; PV, parvalbumin; REM, rapid eye movement sleep; TRN, thalamic reticular nucleus.

This is an open access article under the terms of the [Creative Commons Attribution-NonCommercial](https://creativecommons.org/licenses/by-nc/4.0/) License, which permits use, distribution and reproduction in any medium, provided the original work is properly cited and is not used for commercial purposes.

© 2023 The Authors. *European Journal of Neuroscience* published by Federation of European Neuroscience Societies and John Wiley & Sons Ltd.

Schönauer & Pöhlchen, 2018; Winsky-Sommerer et al., 2008), and the artificial introduction of sleep spindles increases the number of NREM-REM and REM-NREM transitions (Kim et al., 2012).

The TRN is strategically located between the cortex and thalamus, which allows it to exert distinct functions during awake and sleep states. During awake states, the TRN controls selective attention, via its interactions with the sensory thalamic nuclei (Crick, 1984; Halassa et al., 2014; McAlonan et al., 2006). Conversely, during sleep states, TRN activity induces a strong inhibition of the thalamus and participates in sleep spindle production (Halassa & Acsády, 2016; Herrera et al., 2016; Lewis et al., 2015). The role of limbic-projecting TRN neurons during awake states is still unresolved; however, during sleep, they are known to remain silent till arousal (Halassa et al., 2014).

The TRN anteroposterior heterogeneity has been characterized at the anatomic (Crabtree, 1996; Pinault, 2004; Shosaku et al., 1989) and genetic level (Li et al., 2020). According to anatomical studies, the TRN resembles the cortical functional map with two overlapping subsectors: limbic and sensory. All limbic thalamic nuclei not incorporated in the sensory information propagation send fibres to the rostral part of the TRN. In contrast, all thalamic nuclei integrating sensory information are located on the caudal side of the TRN area. Genetically, recent transcriptomic analysis uncovered two subtypes of TRN neurons localized in a similar anteroposterior manner (Li et al., 2020). Despite these recent advances, little is known about the functional role of the anterior and posterior TRN subdivisions on the sleep-wake cycle.

In this study, optogenetic manipulations of the rostral and caudal TRN showed opposite effects on the sleep episode length without affecting overall sleep duration. The caudal TRN had effects on sleep initiation and maintenance, as demonstrated by the fact that its inhibition resulted in rapid awakening and fragmented sleep. On the contrary, the optogenetic silencing of the rostral TRN resulted in prolonged sleep episodes, suggesting a role of this area in arousal. Both debilitating and enhancing effects on sleep architecture caused by TRN manipulation was associated with the reduction of cortical delta (1–4 Hz) and alpha (9–16 Hz) oscillations at distinct sleep stages.

## 2 | RESULTS

### 2.1 | Expression of inhibitory opsins in caudal and rostral TRN

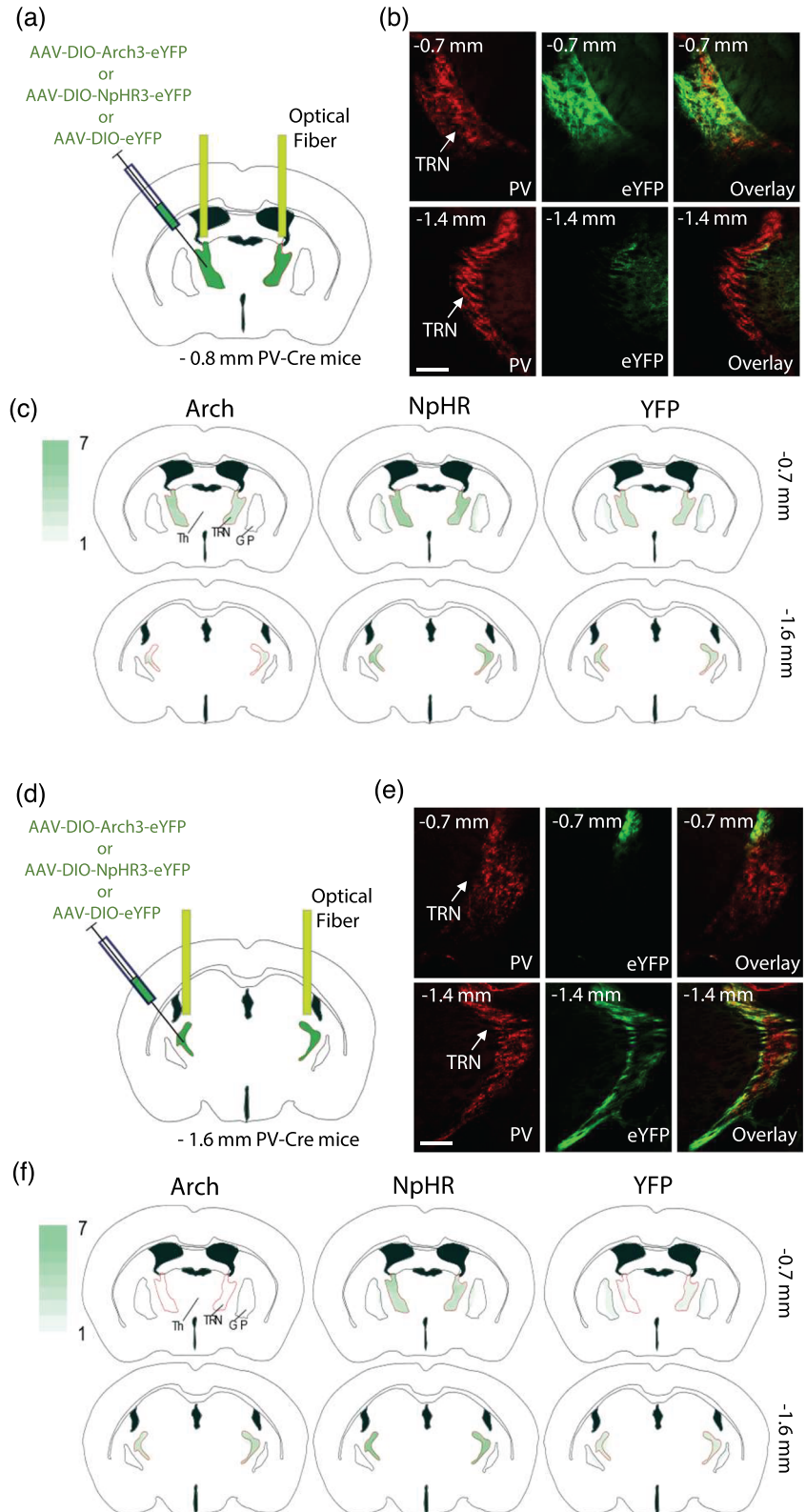
To optogenetically inhibit the rostral and caudal TRN, we expressed inhibitory opsins, archaerhodopsin (Arch) or

halorhodopsin (NpHR), in parvalbumin (PV) containing neurons in the TRN, which account for 80% of all neurons in the TRN (Clemente-Perez et al., 2017; Hou et al., 2016; Steullet et al., 2018). We stereotactically injected an adeno-associated virus (AAV) carrying a Cre-inducible vector encoding either inhibitory opsins or eYFP (control) in the rostral or caudal TRN of PV-Cre mice. Virus injection and bilateral optic fibre placement in rostral mice took place at  $-0.8$  mm from the Bregma on the anteroposterior axis (Figure 1a). In caudal mice the injection was performed at  $-1.6$  mm from the Bregma (Figure 1d). Virus expression in rostral mice was mainly restricted to the rostral TRN and rarely spread to the caudal part of the nucleus (Figures 1b,c and S9). Likewise, caudal TRN showed strong virus expression in caudal mice and little or no virus in the rostral TRN (Figures 1e,f and S9). Optical fibres were placed on top of the virus injection sites.

### 2.2 | Sleep episode duration changes following optogenetic inhibition of caudal and rostral TRN

To examine the role of the caudal and rostral TRN during sleep we used optogenetics combined with cortical EEG recording in freely moving animals (see Section 4). Tonic green light (560 nm, 3 mW) delivery to the TRN through chronically implanted optic fibres was applied in the following pattern: ‘light on’ phase (30 s) followed by ‘light off’ phase (60 or 90 s). Each recording session contained on average 40 cycles of light stimulation (Figure 2a). Additionally, we introduced two sessions of control recordings (Figure 2b), when optic light fibres were not connected to the optic fibre implants on mice head and light did not reach the TRN (No Stim session). All Arch animals slept during No Stim sessions, and unfortunately, only couple of animals from NpHR and Control groups slept during dedicated sessions. An algorithm for sleep state classification was adopted from Halassa et al. (2014) (Figure S1). In general, rostral animals showed non fragmented sleep during Stim sessions (Figure 2c), but caudal animals showed fragmented sleep in Stim sessions compared to No Stim sessions (Figure 2d). Light stimulation in rostral animals expressing inhibitory opsin (Arch and NpHR) introduced tendency to longer sleep episodes, while caudal mice showed the opposite effect, that is fragmented sleep (Caudal Opsin:  $t_3 = 3.736$ ,  $p = 0.033$ ,  $d = 1.868$ ; Rostral Opsin:  $t_3 = 3.711$ ,  $p = 0.034$ ,  $d = 1.856$ ; paired  $t$  test; Figure 2e). During Stim sessions, the sleep episodes of mice expressing Arch and NpHR in the rostral TRN were less fragmented relatively to animals expressing inhibitory

**FIGURE 1** Opsin expression pattern after bilateral AVV targeting in caudally or rostrally injected mice. (a, d) Schematic of the genetic targeting and optic fibre used in stimulation of the rostral (caudal) TRN. AAV-DIO-Arch3-eYFP, AAV-DIO-NpHR3-eYFP or AAV-DIO-eYFP were infused into rostral TRN of the PV-cre mice. (b, e) Virus expression expansion during rostral (caudal) injection. Virus was selective targeting most of the TRN neurons in the rostral (caudal) TRN, and limited fluorescence was detected in the caudal TRN. Scale bar: 250  $\mu$ m. (c, f) Summary diagram of virus expression pattern in the rostrally/caudally injected mice expressing Arch ( $n = 5/4$ ), NpHR ( $n = 5/7$ ) and YFP ( $n = 3/2$ ). Schematic drawings of coronal sections of two coordinates containing the rostral and caudal TRN. Virus expression in the same area for several animals is shown in darker green colour. GP, globus pallidus; Th, thalamus



opsins in the caudal TRN and eYFP (Stim: two-way ANOVA  $F_{2,13} = 6.736$ ,  $p = 0.009$ ; pairwise comparison: Caudal Arch vs. Rostral Arch,  $p = 0.002$ ; Caudal NpHR vs. Rostral NpHR,  $p = 0.007$ ; Rostral Arch vs. Rostral Control,  $p = 0.001$ ; Rostral NpHR vs. Rostral Control,

$p = 0.007$ ; Figure 2f). Synergistic effects for sleep episode comparison were produced by the combination of Arch and NpHR animals into opsin group (Stim: one-way ANOVA  $F_{2,16} = 15.879$ ,  $p = 0.0001$ ; Tukey HSD: Caudal Opsin vs. Rostral Opsin,  $p = 0.0003$ ; Rostral Opsin

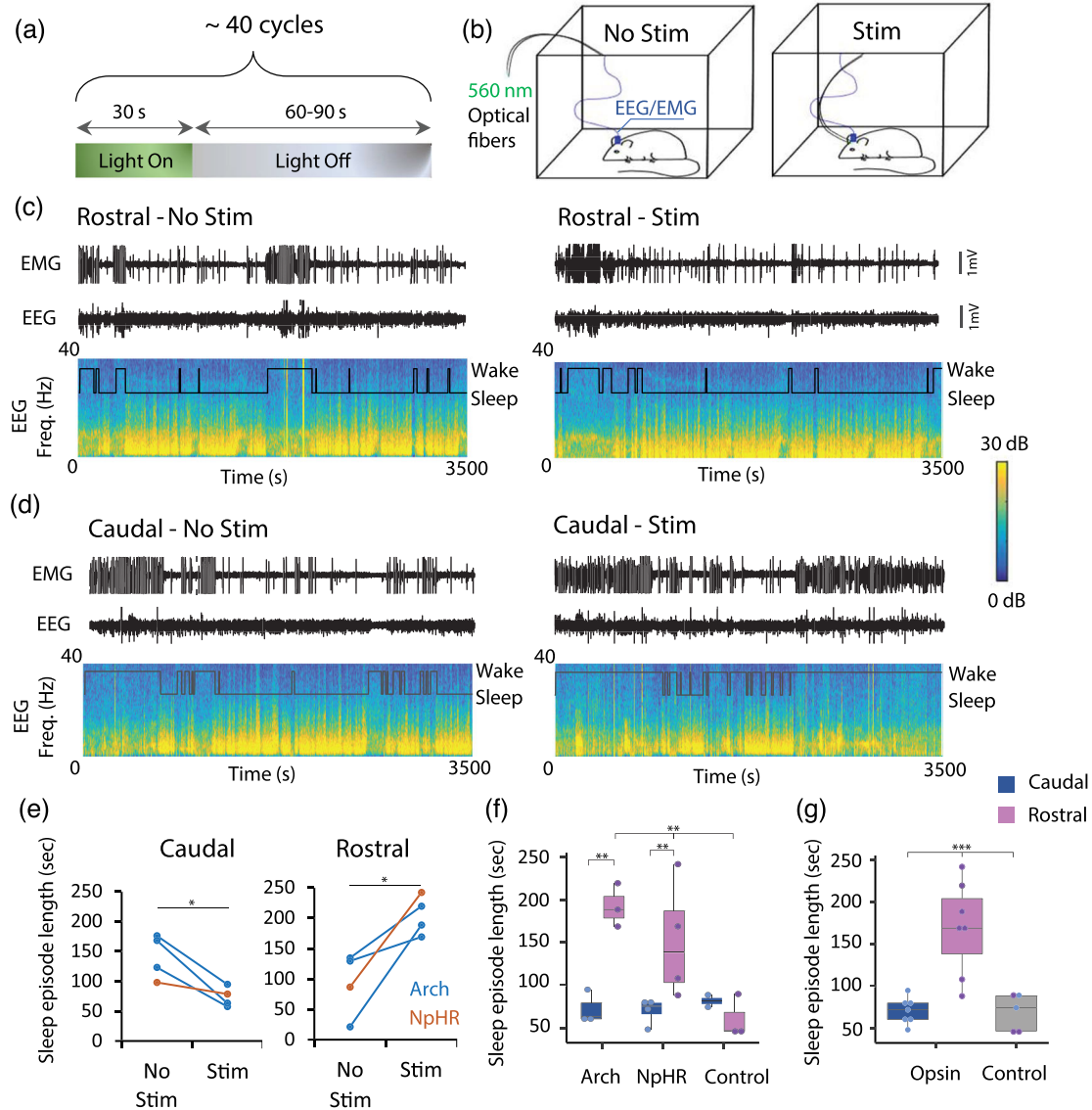


**FIGURE 2** Effect of rostral and caudal TRN inhibition on sleeping episode length. (a) Schematic of the continued light delivery pattern during optogenetic stimulation. The 30 s long light application phase (Light On) was followed by a no light phase, which lasted 60 or 90 s. On average, single experiment consisted of 40 cycles. (b) Schematic representation of the in vivo recording with (Stim) and without (No Stim) light stimulation. During No Stim, optic fibres were disconnected. (c, d) Representative EMG traces, EEG traces and spectrograms from rostral and caudal mice with and without stimulation. Hypnograms are superimposed as black traces on the EEG spectrogram. (e) Average sleep episode length in mice expressing Arch and NpHR in rostral and caudal TRN before and during light application. (f) Average sleep episode length in mice expressing Arch, NpHR and eYFP in the rostral and caudal TRN during light application. (g) Average sleep episode length in mice expressing inhibitory opsin (Arch + NpHR) and eYFP in the rostral and caudal TRN during light application (Arch,  $n = 3/3$ ; NpHR,  $n = 4/4$ ; eYFP,  $n = 3/2$ ). \* $p < 0.05$ ; \*\* $p < 0.01$ ; \*\*\* $p < 0.001$ . One-way ANOVA or paired  $t$  test

vs. Control,  $p = 0.0007$ ; Figure 2g). Light stimulation did not have any effect on the wake episode duration or on total sleep duration in animals expressing inhibitory opsins and eYFP (Figure S2). Overall, we observed opposite effects on sleep quality arising from silencing of different parts of the TRN. These data support distinct functional roles of the rostral and caudal TRN in sleep.

### 2.3 | Caudal TRN activity is important for sleep initiation and maintenance

We confirmed that rostral and caudal optogenetic inhibition of the TRN induced opposite changes to sleep episode duration. Next, we wanted to understand what causes such variations and during which sleep phases these differences arise. First, we investigated the effect of the TRN



optogenetic inhibition on the early sleep. The inclusion criteria for analysis were the following: mice were asleep more than 10 s before light stimulation and woke up within 80 s from the start of the light stimulation (Figure 3a). Caudal mice expressing Arch had a strong linear relationship between sleeping time before light stimulation and the latency to arousal, during light stimulation (Figure 3b–d). If an animal slept less than 20 s prior to stimulation, rapid wake up followed. Such unexpected relationship between early sleep and light stimulation was not observed in rostral Arch-expressing mice, or in NpHR-expressing mice (Figure 3e). When the results of both inhibitory opsins (Arch and NpHR) were combined in Opsin group, the relationship observed in caudal and rostral mice was still maintained (Figure 3f). Surprisingly, the Control group with rostral stimulation showed number of rapid awakenings during stimulation (Figure 3g).

Next, we investigated whether the TRN light stimulation during early sleep (period between 10 to 20 s) and deep sleep (>20 s) had a similar effect on arousal latencies (Figure 4a,b). Light stimulation of caudal TRN had a dramatic effect on the length of latency during early sleep phase. Mice expressing Arch and NpHR in the caudal TRN woke up faster during early sleep stimulation (Arch Caudal: Mann–Whitney  $U$ ,  $U = 168$ ,  $z = -3.372$ ,  $p = 0.0007$ ; NpHR Caudal: Mann–Whitney  $U$ ,  $U = 471$ ,  $z = -2.803$ ,  $p = 0.005$ ; Opsin Caudal: Mann–Whitney  $U$ ,  $U = 1210$ ,  $z = -4.442$ ,  $p = 0.000009$ ; Figure 4c). Control stimulation of caudal TRN did not influence latency to arousal (Control Caudal: Mann–Whitney  $U$ ,  $U = 80$ ,  $z = -1.628$ ,  $p = 0.108$ ; Figure 4c). Only caudal TRN inhibition led to rapid state change during early sleep, as rostral TRN inhibition rarely resulted in the arousal (Arch Rostral: Mann–Whitney  $U$ ,

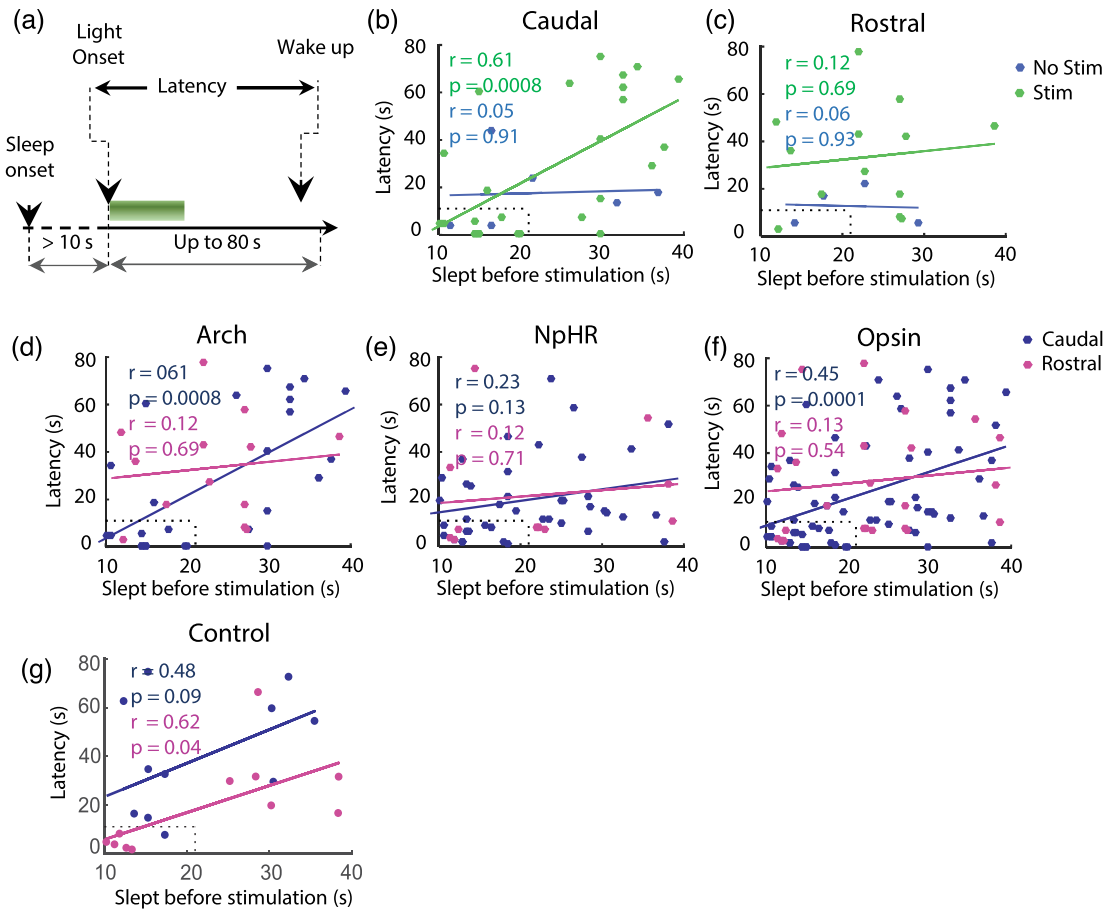


**FIGURE 3** Relationship between sleep length before stimulation and latency to wake. Latency is a time period between the light stimulation start and brain state change (wake). (a) Schematic of the inclusion criteria. Data were included if animal slept more than 10 s before stimulation and woke up within 80 s after light stimulation start. (b, c) The relationship between the sleep duration before stimulation and the latency in rostrally and caudally stimulated animals with (Stim) and without stimulation (No Stim). (d, e, f) The effect of the rostral and caudal light stimulation on relationship between the sleep duration before stimulation and the latency in animals expressing Arch, NpHR, inhibitory Opsin (Arch + NpHR) and Control (eYFP).  $r$ , correlation coefficient,  $p$ , probability value, s, seconds. Arch,  $n = 3/3$ ; NpHR,  $n = 4/4$ ; YFP,  $n = 3/2$

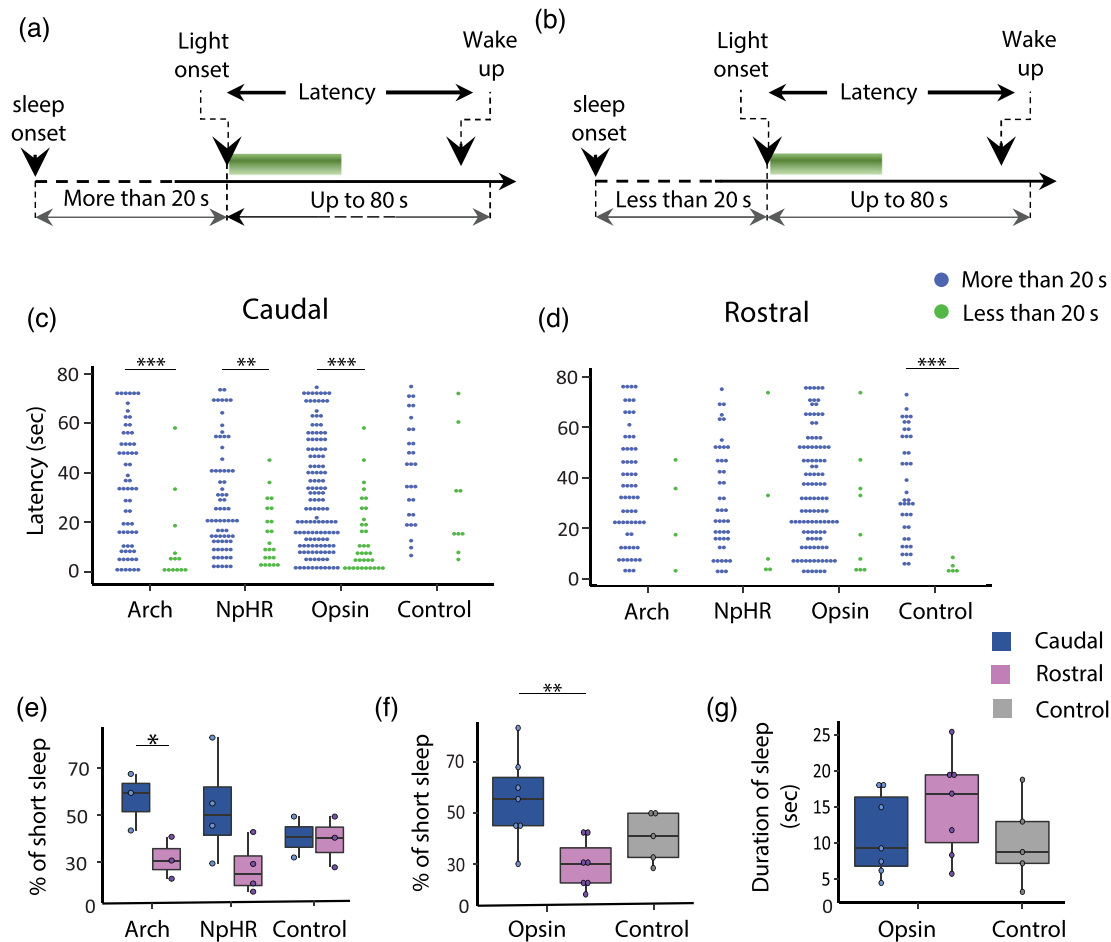


**FIGURE 4** Light stimulation effect during different sleep phases. (a, b) Schematic of the inclusion criteria. Data were included if animal slept more than 10 s before stimulation and woke up within 80 s after light stimulation started. Further, the data were differentiated into two groups depending of the pre-sleep period before stimulation: animals that slept less or more than 20 s prior stimulation. (c) Latencies to arousal in animals expressing Arch, NpHR, Opsin (Arch + NpHR) and YFP (control) in caudal part of the TRN. (d) Latencies to arousal in animals expressing Arch, NpHR, Opsin (Arch + NpHR) and Control (YFP) in rostral part of the TRN. (e) Proportion of the short sleep episodes in animals expressing Arch, NpHR and YFP (control), which sleep more than 20 s before stimulation. (f) Proportion of short sleep episodes in animals expressing opsins (Arch + NpHR) and YFP (control), which sleep more than 20 s before stimulation. (i) Mean sleeping time during 30 s light stimulation episodes. \* $p < 0.05$ ; \*\* $p < 0.01$ , \*\*\* $p < 0.001$ ; (c) Mann–Whitney  $U$ ; (e)  $t$  test; (f) one-way ANOVA

$U = 93$ ,  $z = -0.873$ ,  $p = 0.404$ ; NpHR Rostral: Mann–Whitney  $U$ ,  $U = 83$ ,  $z = -0.954$ ,  $p = 0.359$ ; Opsin Rostral: Mann–Whitney  $U$ ,  $U = 356$ ,  $z = -1.33$ ,  $p = 0.184$ ; Figure 4d). Control stimulation of rostral TRN resulted in rare, but rapid arousal (Control Rostral: Mann–Whitney  $U$ ,  $U = 3$ ,  $z = -3.503$ ,  $p = 0.00001$ ; Figure 4d). We concluded that caudal TRN activity during early sleep is important for sleep initiation, while rostral TRN is not involved.

Next, we wanted to understand the TRN role in the maintenance of deep sleep. If an animal slept more than 20 s before light stimulation (Figure 4a) and woke up within 80 s after stimulation, we labelled it as a short sleep episode. Mice with rostrally inhibited TRN tended

to rarely wake after stimulation, while animals with caudal inhibition woke up in 55% of cases (Arch – Caudal: 57%, three mice vs. Rostral: 32%, three mice,  $t_4 = 2.895$ ,  $p = 0.044$ ; NpHR – Caudal: 53%, four mice vs. Rostral: 28%,  $t_6 = 2.038$ ,  $p = 0.088$ ; Control – Caudal: 41%, two mice vs. Rostral: 40%, three mice,  $t_3 = 0.144$ ,  $p = 0.895$ ; two-tailed  $t$  test; Figure 4e). Both inhibitory opsins showed identical results ( $F_{2,16} = 6.572$ ,  $p = 0.008$ , one-way ANOVA; post hoc: Opsin,  $p = 0.006$ ; Control,  $p = 0.161$ ; Figure 4f). Stimulation during deep sleep induced more fragmented sleep in caudally inhibited mice. The total amount of sleep was not affected by the TRN inhibition ( $F_{2,16} = 1.184$ ,  $p = 0.129$ , one-way ANOVA, Figure 4g). Additionally, the continuous

manner of the light application did not have effect on the latency to wake (Figure S3a,b). In summary, mice with rostrally inhibited TRN had less fragmented sleep and caudal TRN inhibition had more fragmented sleep, as caudal TRN activity appeared to be important for the sleep initiation and maintenance.

## 2.4 | Caudal TRN inhibition during deep sleep led to alpha oscillation power reduction

To examine site-specific effects of optogenetic TRN inhibition on cortical EEGs, we compared different frequency bands before and after the onset of optical stimulation. First, we probed deep sleep oscillations (Figure 5a). We recorded the reduction of EEG powers in several frequency bands, but these were affected only during 10 s of the stimulation (Figure 5b,c). Delta (1–4 Hz) power reduction during 10 s of stimulation was significantly changed for both caudal and rostral animals,  $\chi^2(2) = 7.38$ ,  $p = 0.025$ ,  $\eta^2 = 0.405$ ; Kruskal–Wallis  $H$  test, pairwise comparison; Caudal vs. Control,  $p = 0.008$ ; Rostral vs. Control,  $p = 0.04$ ; Figures 5d and S4a. Alpha (sleep spindle) power (9–16 Hz) was significantly decreased only in the caudally stimulated animals expressing inhibitory opsins ( $F_{2,16} = 4.681$ ,  $p = 0.025$ ;  $\eta^2 = 0.369$ . One-way ANOVA; post hoc: Caudal vs. Control,  $p = 0.021$ ; Rostral vs. Control,  $p = 0.182$ ; Figures 5e and S4b). Additionally, we employed paired  $t$  test analysis to compare the power spectra derived from EEG traces 10 s before and during the 10 s light stimulations. Caudal TRN inhibition demonstrated a reduction in the alpha power oscillation (Alpha,  $p = 0.04$ ; Delta,  $p = 0.217$ , paired  $t$  test; Figures S5 and S6). Rostrally inhibited TRN did not induce any difference in alpha and delta oscillations over 10 s stimulation (Alpha,  $p = 0.39$ ; Delta,  $p = 0.166$ , paired  $t$  test; Figures S5 and S6). Although, a brief, 5 s long, delta oscillation reduction was recorded in caudal and rostral animals expressing inhibitory opsins (Caudal – Delta,  $p = 0.031$ ; Rostral – Delta,  $p = 0.006$ ; Figure S6). Light stimulation in caudal and rostral TRN of control animals did not have any effect on alpha and delta oscillation powers (Caudal – Alpha,  $p = 0.58$ ; Delta,  $p = 0.08$ . Rostral – Alpha,  $p = 0.12$ ; Delta,  $p = 0.05$ , paired  $t$  test; Figures S5 and S6). Rostral light stimulation in control mice induced delta power increase during sleep ( $p = 0.05$ , paired  $t$  test; Figure S6). Continuous light stimulation did not introduce any additive effect on the oscillation power reduction (Figure S3c–e).

The fact that the sleep spindle oscillation (9–16 Hz) was reduced in caudal animals expressing inhibitory

opsins underlies the idea that the sleep spindle events should be affected too. An algorithm for sleep spindle events detection was adopted from Halassa et al. (2014) (Figure S7). We recorded a reduction of sleep spindle events in caudal animals over 12 s of the stimulation (Caudal Opsin:  $t_9 = 2.374$ ,  $p = 0.042$ ,  $d = 0.751$ ; Rostral Opsin:  $t_7 = 1.152$ ,  $p = 0.287$ ,  $d = 0.407$ ; Control:  $z = 0.944$ ,  $p = 0.345$ . Paired  $t$  test or Wilcoxon signed rank test; Figure 5f).

Overall, rostral and caudal TRN optogenetic inhibition over 10 s resulted in delta oscillation reduction, but only caudal TRN inhibition was associated with alpha power and spindle events decrease. Control light stimulation in rostral TRN slightly increased the delta power.

## 2.5 | Rostral TRN inhibition during pre-wake sleep led to alpha and delta oscillation power reduction

Next, we analysed the pre-wake traces, during which animals were asleep at least 20 s before stimulation, 10 s during stimulation and then woke up in the period of 80 s after stimulation (Figure 6a). The overall power reduction for alpha and delta oscillation balance shifted relative to deep sleep phases. In the pre-wake stage, the strongest power reduction was recorded in animals with rostrally inhibited TRN (Figures 6b and S8b). Inhibition of both parts of the TRN induced visible power reduction on spectrograms (Figures 6c and S8c), but in pre-wake sleep the significant change in alpha and delta reduction was recorded only in the rostrally inhibited TRN (Caudal – Alpha,  $p = 0.106$ , Delta,  $p = 0.066$ ; Rostral – Alpha,  $p = 0.015$ , Delta,  $p = 0.012$  paired  $t$  test; Figures 6d and S8d). Lewis et al. (2015) optogenetically stimulated caudal TRN and recorded significant increases in delta oscillations. Our control light stimulation of rostral TRN had a similar tendency to increase delta power during sleep, but contrary to the Lewis et al.'s study, it was associated with rise in beta-gamma power (15–50 Hz) ( $p = 0.02$ , paired student  $t$  test; Figures 6f and S8f).

To summarize, the pre-wake sleep oscillation inhibition balance shift was marked by a significant drop in delta and alpha power during optogenetic inhibition of rostral TRN.

## 2.6 | Alpha oscillation reduction is correlated with wake-up latency in animals with caudally inhibited TRN

Lastly, we wanted to understand which oscillation band power reduction, caused by the TRN optogenetic

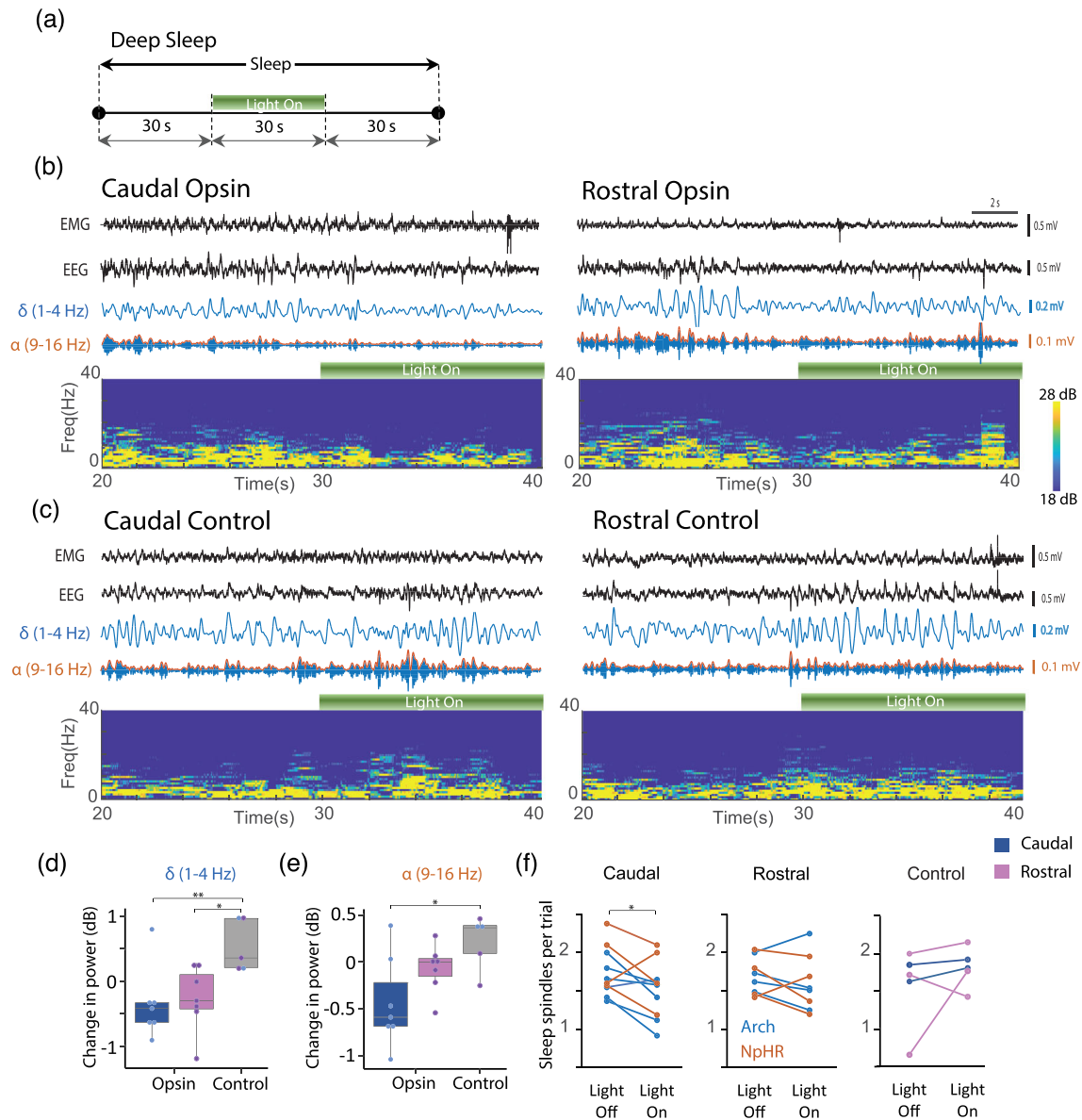


**FIGURE 5** Effect of tonic optogenetic inhibition on delta and alpha band EEG power and sleep spindles during deep sleep. (a) Schematic of the inclusion criteria. Data were included for analysis and named as a deep sleep if animal slept at least 30 s before stimulation and did not woke up within 60 s after light stimulation start. (b) Representative EMG, EEG, filtered delta (1–4 Hz) and alpha (9–16) traces and the corresponding heat map EEG power spectrum illustrating behavioural response to optogenetic silencing in animals expressing inhibitory opsins in caudal (left) and rostral (right) TRN. (c) Representative EMG, EEG, filtered delta (1–4 Hz) and alpha (9–16) traces and the corresponding heat map EEG power spectrum illustrating behavioural response to light stimulation in animals expressing eYFP in caudal (left) and rostral (right) TRN. (d) Quantification of the delta power (1–4 Hz) change during first 10 s of the optogenetic silencing in animals expressing inhibitory opsin (Arch or NpHR) and eYFP. (e) Quantification of the alpha power (9–16 Hz) change during first 10 s of the optogenetic silencing in animals expressing inhibitory opsin (Arch or NpHR) and eYFP. (f) Number of detected sleep spindles events per trial before and during light stimulation in animals expressing inhibitory opsins (Arch or NpHR) and eYFP in caudal and rostral TRN. \* $p < 0.05$ ; \*\* $p < 0.01$ ; one-way ANOVA or paired  $t$  test

oscillation, is correlated with arousal latency. Inclusion criteria for this analysis was identical to the pre-wake traces collection, where the animal slept at least 20 s before stimulation and at least 10 s during stimulation to calculate EEG power difference (Figure 7a). Only caudally stimulated Arch-expressing animals showed strong,

positive correlation between alpha oscillation change during first 10 s of stimulation and the arousal latency (Figure 7b). Rostrally stimulated Arch animals during pre-wake did have significant reduction in the alpha oscillation power ( $p = 0.01$ , paired  $t$  test), but this was not related to wake-up latency (Figure 7b). Neither group of NpHR-



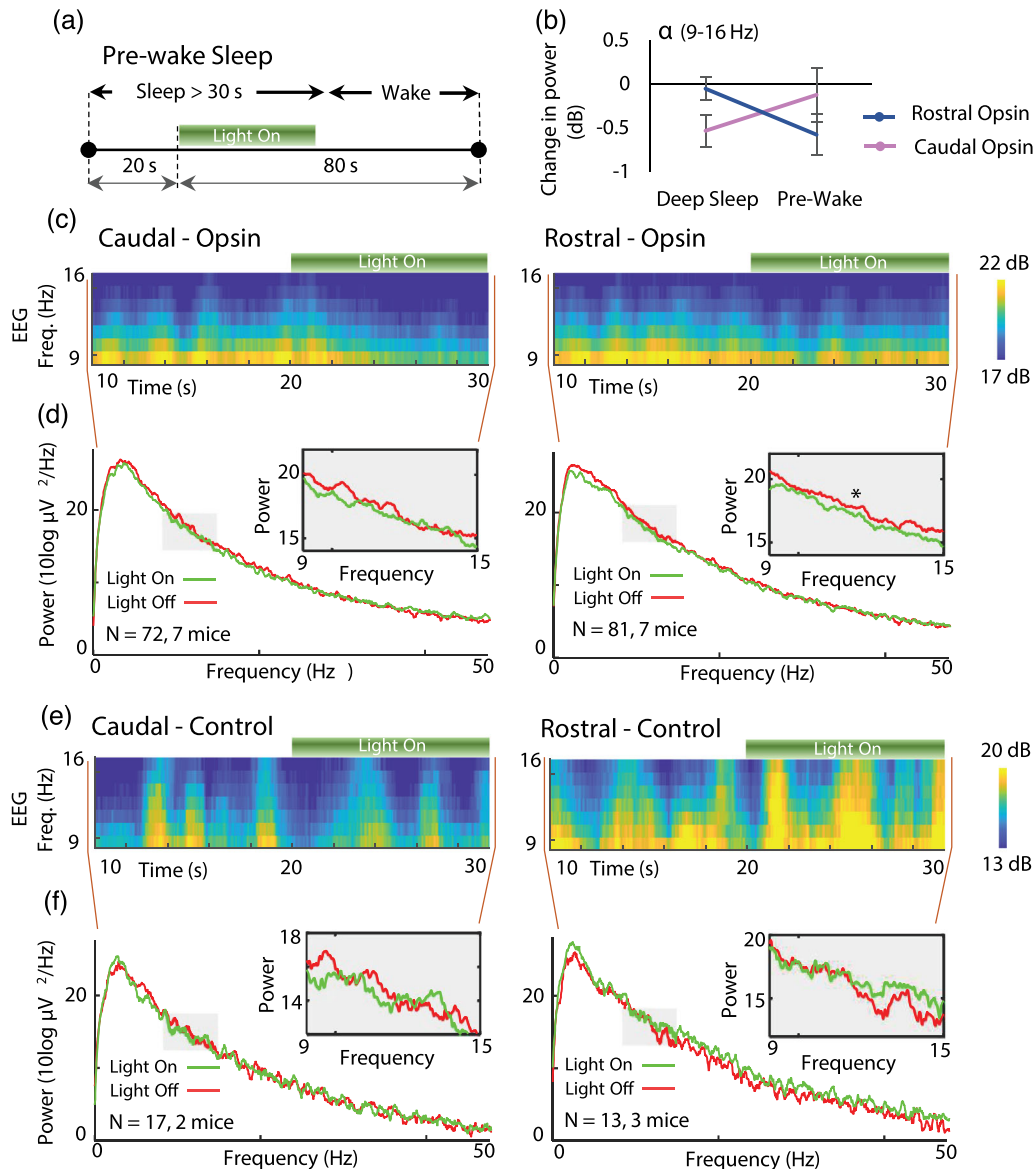


**FIGURE 6** Effect of tonic optogenetic inhibition on alpha band EEG power during pre-wake sleep. (a) Schematic of the inclusion criteria. Data were included for analysis and named as a pre-wake sleep, if animals woke up during 80 s after light stimulation starts. In addition, animals were supposed to sleep at least 20 s before stimulation and 10 s during light stimulation. (b) Comparison of the alpha power (9–15 Hz) change during deep sleep and pre-wake sleep. The power changes used for the comparison were recorded during first 10 s of the optogenetic silencing in animals expressing opsins (Arch or NpHR) in the TRN. (c) Spectrograms are showing average effect on the alpha band power for 10 s light stimulation in animals expressing inhibitory opsins in caudal (left) and rostral (right) TRN. (d) Average spectrum of the 10 s before and 10 s during light stimulation in animals expressing inhibitory opsins. Grey region shows zoomed-in plot of the alpha band spectrum. (e) Spectrograms are showing average effect on the alpha band for 10 s light stimulation in animals expressing inhibitory YFP in caudal (left) and rostral (right) TRN. (f) Average spectrum of the 10 s before and 10 s during light stimulation in animals expressing YFP. Grey region shows zoomed-in plot of the alpha band spectrum. \* $p < 0.05$ ; paired  $t$  test

expressing mice showed significant correlation with latency (Figure 7c). We did not observe synergistic statistical empowerment when we combined the Arch and NpHR groups and correlation was reduced in caudally stimulated animal (Figure 7d). Alpha power change did not relate to the arousal latency in control animals (Figure 7e).

Reduction of the alpha oscillation in caudally targeted animals is related to the fragmented sleep, while the reduction of the alpha power in rostral part of the TRN does not speed up wake up and putatively can prolong sleep during pre-wake period.

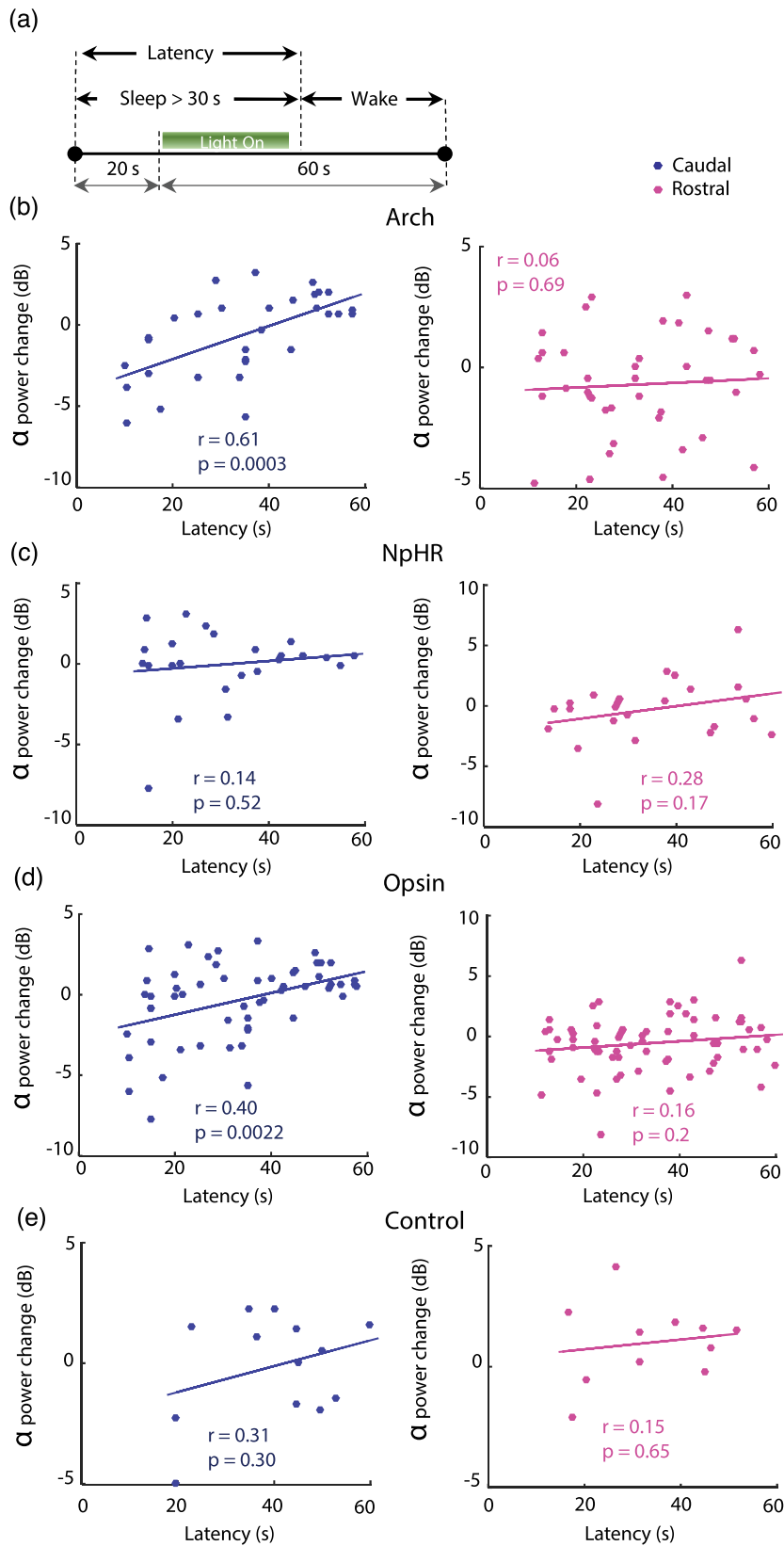


**FIGURE 7** Correlation of the alpha power reduction with the latency to wake up. (a) Schematic of the inclusion criteria. Data were included for analysis, if animals woke up during 60 s after light stimulation starts. In addition, animals were supposed to sleep at least 20 s before stimulation and 10 s during light stimulation. (b, c, d, e) Correlation of the alpha power reduction during 10 s of light stimulation with latency to wake up in animals expressing Arch, NpHR, Opsin and YFP (control).  $r$ , correlation coefficient,  $p$ , probability value

### 3 | DISCUSSION

We showed that optogenetic silencing of caudal and rostral TRN had opposed effects on the sleep architecture.

Caudal inhibition of the TRN introduced fragmented sleep, while rostral TRN inhibition promoted sleep bout prolongation. Optogenetic inhibition of both areas led to reduction of the delta and alpha cortical

oscillations during distinct sleeping stages. Current characterization of the TRN subpopulation activity during various sleeping stages would allow a better understanding of thalamocortical interactions during sleep and anaesthesia.

The TRN is a non-homogenous structure containing sensory and limbic projecting neurons, which can fire in a state-dependent manner (Halassa et al., 2014). In the present study, we characterized the impact of optogenetic inhibition of two TRN subpopulation on the sleep architecture and showed that the activity shift to the caudal TRN is important for sleep initiation and maintenance, while the pre-wake sleeping stage is characterized by an activity shift to the rostral TRN. Recently, two TRN subpopulations were characterized to quantitatively distribute in an anterior posterior manner. Dysfunction in the posteriorly (caudally) located TRN cells, which project to sensory thalamic nuclei, results in reduction of delta oscillation, sleeping spindles and NREM sleep bouts (Li et al., 2020). Likewise, optogenetic inhibition of the posterior TRN in our case resulted in reduced sleeping episodes, alpha and delta oscillations during deep sleep stages. We also showed that inhibition of the rostral TRN leads to reduction in the alpha and delta oscillations, which putatively promotes less fragmented sleep. It has been shown that altered neuronal firing in the TRN can result in frequent or prolonged brain state transitions (Astori et al., 2011; Kim et al., 2012). Thus, TRN distinct subnetworks are involved in the initiation, maintenance, and termination of local sleep.

The area of the TRN that is involved in NREM-REM transitions is still unresolved. One caveat of our approach is the low sensitivity to small REM traces during analysis of deep and pre-wake sleep. It is important to note that a previous study on TRN modulation during REM sleep did not introduce any changes in EEG oscillation or sleep quality (Herrera et al., 2016).

The alpha oscillation reduction caused by optogenetic inhibition of caudal TRN resulted in fragmented sleep and was correlated with the latency to arousal. The sleep spindle malfunction leads to the altered sleep cycle (Kim et al., 2012; Ni et al., 2016; Wells et al., 2016; Wimmer et al., 2012). The short timescale of the oscillation reduction (10 s) could be caused by the photocurrent decline characteristics for Arch and NpHR opsins and light induced heating. It is important to note that recorded sleep spindle event decrease can act as reflection of the sleep spindles' amplitude reduction.

We used two inhibitory opsins with different hyperpolarization mechanisms to silence neurons, and therefore, we expected them to yield different results (Chow et al., 2010; Zhang et al., 2007). EEG power modulation and sleep/wake cycle effect were almost identical for the

two inhibitory opsins used, but the effect on the latency to wake up was significant only in Arch-expressing mice. We hypothesize that Arch light stimulation led to a stronger neuronal inhibition relative to NpHR, as all mice were stimulated at optimal wavelength for Arch (525 nm, green), but not for NpHR (593 nm, yellow).

Sleep spindles were recorded and named 'alpha' waves more than 90 years ago, but we are still far from complete understanding of their physiological role (Lüthi, 2014; Práwdicz-Neminski, 1925). As the subproduct of the TRN neuronal bursting discharge, the neural circuits responsible for these waves were characterized in rodents based on the neurochemistry (Clemente-Perez et al., 2017), cortical location (Kim et al., 2015), and interconnection with thalamic nuclei (Clemente-Perez et al., 2017; Fernandez et al., 2018). The large cortical area in humans allowed the topographical organization of fast (~12 Hz) and slow (~14 Hz) sleep spindles to be distinguished, with a sharp border in the supplementary motor area (Andrillon et al., 2011). Current methodologies fail to differentiate fast and slow spindles in mice, but the sensory TRN neurons have been shown to be capable of stronger repetitive burst discharge relatively to limbic TRN areas due to higher activity of the low-threshold  $Ca^{2+}$  channel  $Ca_v3.3$  (Fernandez & Lüthi, 2020; Fernandez et al., 2018; Li et al., 2020). This suggest that mice have at least two types of sleep spindles generated by different circuitries (Li et al., 2020). According to our data, caudal and rostral TRN could be generating alpha oscillations in mouse cortex at different sleeping periods. Thereby, the distinct sleep spindles might be further differentiated based on the temporal resolution and functionality. Future studies addressing sleep spindle mechanisms should consider the location of the targeted TRN subsector and the sleep stages during which spindles are produced.

Tonic activation of the TRN induced slow wave activity in awake animals (Lewis et al., 2015). Conversely, in our hands, tonic inhibition in the awake states did not produce any detectable changes on EEG oscillation. During the wake state, thalamic neurons have higher membrane potential levels, and the TRN neurons exhibit weaker inhibitory control, as they fire in tonic manner and can only amplify chosen cortical inputs without modulation of their content (Halassa & Acsády, 2016). Thus, the optogenetic inhibition of the TRN during the awake state does not have a pronounced effect on the global EEG oscillations, but still has obvious consequences on behaviour (Clemente-Perez et al., 2017; Halassa et al., 2014). Additionally, the modulation of the TRN activity did not affect global sleep length, as it might act as part of the circuit for arousal control across only local cortical areas (Fernandez et al., 2018; Lewis

et al., 2015), through which the brainstem, hypothalamus and basal forebrain can control the forebrain arousal state activity (Buzsaki et al., 1988; Herrera et al., 2016; Kolmac & Mitrofanis, 1998).

A limitation of the current study is that a relatively small number of control animals slept during recording session. In vivo electrophysiological recording during light application would be an interesting addition to the study. However, we can predict that in vivo recording during TRN optogenetic inhibition would not generate a straightforward result as the TRN is a complex structure with a highly interconnected neuronal network (Pinault, 2004). Previously it has been shown that tonic optogenetic activation of the caudal TRN neurons exhibited heterogeneous changes in firing rates, as the majority of TRN cells showed decreased firing rate (Lewis et al., 2015).

Overall, we concluded that rostral and caudal TRN consist of distinct subnetworks, which have different activity levels during sleep. The caudal segment of TRN is important for sleep initiation and maintenance, while the activation of the rostral TRN is linked to sleep cessation. We described the TRN functional heterogeneity by using location principles and highlight that the optogenetic targeting of the TRN segments in future should be taken into account during the design of novel optogenetic experiments.

## 4 | MATERIALS AND METHODS

### 4.1 | Animals

Ten- to sixteen-week-old female (5) and male (19) C57BL/6 mice expressing Cre recombinase in parvalbumin-expressing neurons (PV-Cre) were used ( $n = 24$ ). Animals were housed under standard conditions, with food and water ad libitum. All work was approved by the University of Strathclyde Ethical Review Committee and performed under license in accordance with UK legislation as defined in the Animals (Scientific Procedures) Act 1986.

### 4.2 | Viral vectors and injections

For opsin expression, archaerhodopsin (AAV5-Ef1a-DIO-eArch3.0-EYFP), halorhodopsin (AAV5-Ef1a-DIO-eNpHR3.0-EYFP) and YFP only (AAV5-Ef1a-DIO-EYFP) viruses were used. Viruses were purchased from Vector Core (University of North Carolina) with titres around  $10^{12}$  VG/ml. These viruses were injected bilaterally at volumes of 200–600 nl into the TRN of PV-Cre mice using a

Nanoliter (WPI). Different mice were used for rostral (A/P,  $-0.8$  mm;  $\pm$ M/L,  $1.4$  mm; D/V,  $-3.2$  mm,  $-3.5$  mm,  $-3.8$  mm) and caudal (A/P,  $-1.6$  mm;  $\pm$ M/L,  $2.2$  mm; D/V,  $-3.2$  mm,  $-3.5$  mm,  $-3.8$  mm) TRN targeting. In order to express opsins in TRN in dorsoventral coordinate, virus was injected in 3 different dorsoventral coordinates. Mice were given at least 4 weeks of recovery following surgery to allow virus expression.

### 4.3 | Stereotaxic surgery

Mice were anaesthetized with 5% isoflurane and maintained at 1.5–2%. Five stainless-steel screws were placed in frontal (A/P,  $+2.0$  mm;  $\pm$ M/L,  $1.0$  mm) parietal (A/P,  $-3.0$  mm; M/L,  $4.0$  mm) and cerebellar (ground) parts of the skull. The EEG recorded from frontal screws were used for analysis. The EMG wire was placed in the neck muscle. A pipette filled with virus was lowered at the rate of 500–1000  $\mu$ m/min. The virus was injected at the rate of 25–50 nl per minute using nanoliter (WPI). The virus injection was performed in three coordinates of dorsoventral axis. After each injection, the pipette remained in the brains at least for 5 min to ensure diffusion into the target area. Optic fibre implants (Thorlabs lab, 0.39 NA) were placed in the brain at the depth of 2.7 mm. Kwik-Sil (WPI) was used to cover an interface between open brain area and the skull, and the dental cement was applied to hold the optic fibre implants stable. The cement mixed with black ink were used to cover the light propagation.

### 4.4 | Optical stimulation

Archaerhodopsin, halorhodopsin and YFP expressing neurons were stimulated with a Plexon LED Modules (Plexon, USA) with a wavelength of 525 nm. The light delivery method was adopted from Lewis et al. (2015). Briefly, a 30 s stimulation was followed by a 60–90 s off period. Light intensity was maintained at constant levels throughout a single 30 s period. Simulations for the transmission of light through tissue were performed using the calculator developed by the Deisseroth lab (<http://web.stanford.edu/group/dlab/cgibin/graph/chart.php>). The light intensity at the tip of the optic fibre was  $\sim 300$  mW/mm<sup>2</sup> for all recordings. Halorhodopsin light stimulation had gradual ramping of the light intensity at the end of the signal, to exclude electrophysiological artefacts induced by chloride pump after sharp deactivation. Recording sessions were limited to no more than 60 stimulation trials to prevent habituation effects.



## 4.5 | Electrophysiology

Four weeks after viral infections, the mice were transferred daily to the recording chamber to acclimate. Recording chamber consisted of one or two plastic, black boxes (50 cm [W], 25 cm [D], 25 cm [H]) inserted in a custom-made Faraday cage. During the habituation session, a mouse was connected to the EEG–EMG cable. Cables were flexible and the mouse was able to move around in the recording chamber. Each chamber contained material for nest building. Electrophysiological recording sessions typically lasted for 2 h. The connectors on the skull were connected through a custom-made adaptor to an Intan Technologies amplifier RHD 2132 board which amplified EEG and EMG signals 1000 times. The amplified signal was sent to the Intan evaluation board where it was further processed. RHD2000 Interface software was used to monitor, and store recorded EEG/EMG signals. The EEG and EMG data were acquired at 1 kHz sampling rate.

## 4.6 | Immunohistochemistry

To reach terminal anaesthesia, pentobarbital/lidocaine mixture (50/50) was injected intraperitoneally ( $\geq 200$  mg/kg). After complete loss of reflexes, the mouse was attached to a board, and the ribcage was opened. It was intracardially perfused using 25 ml of PBS and 25 ml 4% paraformaldehyde solution (PFA) in PBS. Brains were removed and placed in the 4% PFA for 24 h at 4 degrees. On the next day, the brains were moved to a 30% sucrose in PBS for at least 48 h before sectioning.

Sucrose cryoprotected brains were placed in the microtome Leica where they were frozen using dry ice. The brains were cut into 50  $\mu\text{m}$  sections and placed in wells filled with PBS. After three washes (10 min each) with PBS the incubation was performed at room temperature in PBS containing 0.3% Triton X-100 and 1–2% normal donkey serum (PBSX solution). Primary antibody against PV (P3088; Sigma) was diluted at 1/2500 with PBSX solution and applied to brain slices. Well plates were left on the shaker overnight. After several washes with PBS, the sections were incubated for 2–4 h with a mixture of secondary antibody (Alexa Fluor 594; A-11005; Invitrogen; 1:200) with PBSX solution. Sections were mounted on the glass slides covered by Vectashield Hard Set (Vector Labs) and a cover slip placed on them.

The sections were observed using an upright epifluorescent microscope (Nikon, Eclipse E600). The digital images were captured using MetaMorph. Photoshop (Adobe Inc) was used to quantify the number of pixels produced by parvalbumin staining (red) and opsin

expression (green). The percentage of opsin expression was quantified by division of the numbers of pixels produced by opsins and parvalbumin. In the cases when the number of green pixels were higher than number of red pixels, the proportion of pixels was reduced to 100%.

## 4.7 | Data analysis

### 4.7.1 | Sleep state classification

All data was analysed offline with MATLAB (Mathworks). For behavioural state analysis, an algorithm was adopted from Halassa et al. (2014). We classified EEG traces into two states: wake and sleep (majority of which was expected to consist of slow-wave-sleep) using EMG recording. EMG data were filtered from 60 to 200 Hz and threshold were applied. The algorithm, by going through the EEG/EMG data in 5 s steps, detected brain state for each step. Minimum criteria for sleep was at least 15 s duration. Threshold was detected by visual examination and was identical for all animals ( $\text{thr} = 5$ ). The wake trace was identified by higher value than the threshold and sleep trace had lower values than imposed EMG threshold (Figure S1). The sleep scoring was done in a semiautomatic way using custom written MATLAB algorithms. Visual inspection was used to discard putative sleeping trials with low slow/delta oscillation, non-characteristic for slow wave oscillation. Proportionally, a small number of the time segments not related to sleep or wake states were not used in the analysis.

### 4.7.2 | Detection of sleep spindles

An algorithm for detection of sleep spindles was adopted from Halassa et al. (2014). The EEG trace was filtered for 9–16 Hz frequency and transformed with Hilbert transformation. The envelope of signal (1 s smoothing) was used as a basis for spindle detection. A threshold was calculated as a sum of mean and one standard deviation. The threshold was calculated for each trace from the trace area not used for spindle collection (Light Off/Light On). Each threshold crossing, with parameters of  $>0.5$  s and  $<3$  s, was counted as a sleep spindle event (Figure S7). Bins of 12 s before (Light Off) and during (Light On) light stimulation were used to collect sleep spindles for calculation of the overall number of sleep spindles. Sleep spindles per trial were calculated by division of the overall number of sleep spindles over the number of EEG traces. A window of 12 s was used to collect all sleep spindles events over 10 s, as sleep spindle event could last up to 3 s.

### 4.7.3 | EEG spectral analysis

Before spectral analysis, each recording was chunked based on the inclusion criteria (pre-sleep, pre-wake sleep, deep sleep) and checked for artefacts. If the EEG trace contained a peak higher or lower than 800  $\mu\text{V}$ , it was discarded. Power spectral density of each EEG trace was estimated with the Chronux toolbox (<http://chronux.org/>) using 19 tapers over 5 or 10 s windows. Delta range (1–4 Hz) was taken from Lewis et al. (2015) as the design of the study was almost identical. Alpha or spindle frequency was introduced as range of 9–16 Hz; this is in line with a recent article on sleep spindles Fernandez et al. (2018). Mean power spectral density was computed per animal before computing group average. Mean spectrograms were computed per animal before averaging group spectrograms with 5 tapers in 1 s sliding window with 0.01 s steps. Same tapers, moving windows and steps were used for calculation of the single representative spectrograms. Single strong outliers from opsin group were removed in Figures S5 and S6 for demonstration purposes. Outliers remained for statistical analysis and quantification. The codes used and processed data can be found on <https://github.com/Vladimir8585/TRN-project>. Raw data will be provided per request.

### 4.8 | Statistical analysis

To assess the effects of optogenetic stimulation on brain oscillations, each trial data from a 10 s period of stimulation was compared to that of 10 s pre-stimulation for each experimental group using Student's paired *t* test. To compute power spectral change for each animal, the power spectral difference for each trial was derived by subtraction of a 10 s pre-stimulation from a 10 s period of stimulation. Then, the power spectral change for each animal was used to derive the power change for each group. To compare differences between groups with different targeted areas (caudal or rostral) and viruses (archaerhodopsin, halorhodopsin and YFP), two-sample *t* test, and one-way ANOVA were employed (SPSS, IBM). To test normality Shapiro–Wilk test was employed. Kruskal–Wallis, Mann–Whitney *U* and Wilcoxon signed rank tests were used for data which failed normality test. To quantify the effect of the green light stimulation on the sleep/wake cycle two terms were used: latency and the ratio of wake/sleep. The latency is a period from light stimulation starting point until the brain state change. The ratio of short sleep was calculated the following way: the number of stimulation trial with sleep episodes shorter than 80 s were divided on sum of the trial numbers with short (<80 s) and long (>80 s) sleeping

episodes. Pearson correlations were used to measure the linear relationship between latencies and the power changes.

### ACKNOWLEDGEMENTS

We are grateful for the editorial assistance of the NIH Fellow Board during preparation of the paper. The study was founded by the BBSRC industrial CASE PhD Studentship with AstraZeneca partnership.

### CONFLICT OF INTEREST

None to declare.

### AUTHOR CONTRIBUTIONS

**Vladimir Visocky:** Investigation; writing-original draft. **Brian Morris:** Conceptualization; supervision; funding acquisition; writing-review and editing. **John Dunlop:** Project administration; funding acquisition. **Nicholas Brandon:** Project administration; funding acquisition. **Shuzo Sakata:** Conceptualization; supervision; funding acquisition; writing-review and editing. **Judith Pratt:** Conceptualization; supervision; funding acquisition; writing-review and editing.


### PEER REVIEW

The peer review history for this article is available at <https://publons.com/publon/10.1111/ejn.15908>.

### DATA AVAILABILITY STATEMENT

Data will be made available in response to email requests made to the corresponding author.

### ORCID

Vladimir Visocky  <https://orcid.org/0000-0003-1356-588X>

Shuzo Sakata  <https://orcid.org/0000-0001-6796-411X>

### REFERENCES

- Andrillon, T., Nir, Y., Staba, R. J., Ferrarelli, F., Cirelli, C., Tononi, G., & Fried, I. (2011). Sleep spindles in humans: Insights from intracranial EEG and unit recordings. *Journal of Neuroscience*, 31(49), 17821–17834. <https://doi.org/10.1523/JNEUROSCI.2604-11.2011>
- Astori, S., Wimmer, R. D., Prosser, H. M., Corti, C., Corsi, M., Liaudet, N., Volterra, A., Franken, P., Adelman, J. P., & Lüthi, A. (2011). The Ca v3.3 calcium channel is the major sleep spindle pacemaker in thalamus. *Proceedings of the National Academy of Sciences of the United States of America*, 108(33), 13823–13828. <https://doi.org/10.1073/pnas.1105115108>
- Batini, C., Moruzzi, G., Palestini, M., Rossi, G. F., & Zanchetti, A. (1958). Persistent patterns of wakefulness in the pretectal midpontine preparation. *Science*, 128(3314), 30–32. <https://doi.org/10.1126/science.128.3314.30-a>
- Buzsaki, G., Bickford, R. G., Ponomareff, G., Thal, L. J., Mandel, R., & Gage, F. H. (1988). Nucleus basalis and thalamic

- control of neocortical activity in the freely moving rat. *Journal of Neuroscience*, 8(11), 4007–4026. <https://doi.org/10.1523/jneurosci.08-11-04007.1988>
- Chow, B. Y., Han, X., Dobry, A. S., Qian, X., Chuong, A. S., Li, M., Henninger, M. A., Belfort, G. M., Lin, Y., Monahan, P. E., & Boyden, E. S. (2010). High-performance genetically targetable optical neural silencing by light-driven proton pumps. *Nature*, 463(7277), 98–102. <https://doi.org/10.1038/nature08652>
- Clemente-Perez, A., Makinson, S. R., Higashikubo, B., Brovarney, S., Cho, F. S., Urry, A., Holden, S. S., Wimer, M., Dávid, C., Fenno, L. E., Acsády, L., Deisseroth, K., & Paz, J. T. (2017). Distinct thalamic reticular cell types differentially modulate normal and pathological cortical rhythms. *Cell Reports*, 19(10), 2130–2142. <https://doi.org/10.1016/j.celrep.2017.05.044>
- Crabtree, J. W. (1996). Organization in the somatosensory sector of the cat's thalamic reticular nucleus. *Journal of Comparative Neurology*, 366(2), 207–222. [https://doi.org/10.1002/\(SICI\)1096-9861\(19960304\)366:2<207:AID-CNE2>3.0.CO;2-9](https://doi.org/10.1002/(SICI)1096-9861(19960304)366:2<207:AID-CNE2>3.0.CO;2-9)
- Crick, F. (1984). Function of the thalamic reticular complex: The searchlight hypothesis. *Proceedings of the National Academy of Sciences of the United States of America*, 81(14 I), 4586–4590. <https://doi.org/10.1073/pnas.81.14.4586>
- Fernandez, L. M. J., & Lüthi, A. (2020). Sleep spindles: Mechanism and functions. *Physiological Reviews*, 100(2), 805–868. <https://doi.org/10.1152/physrev.00042.2018>
- Fernandez, L. M. J., Vantomme, G., Osorio-Forero, A., Cardis, R., Béard, E., & Lüthi, A. (2018). Thalamic reticular control of local sleep-in mouse sensory cortex. *eLife*, 7, e39111. <https://doi.org/10.7554/eLife.39111>
- Halassa, M. M., & Acsády, L. (2016). Thalamic inhibition: Diverse sources, diverse scales. In *Trends in neurosciences* (Vol. 39, Issue 10, pp. 680–693). Elsevier Ltd. <https://doi.org/10.1016/j.tins.2016.08.001>
- Halassa, M. M., Chen, Z., Wimmer, R. D., Brunetti, P. M., Zhao, S., Zikopoulos, B., Wang, F., Brown, E. N., & Wilson, M. A. (2014). State-dependent architecture of thalamic reticular subnetworks. *Cell*, 158(4), 808–821. <https://doi.org/10.1016/j.cell.2014.06.025>
- Halassa, M. M., Siegle, J. H., Ritt, J. T., Ting, J. T., Feng, G., & Moore, C. I. (2011). Selective optical drive of thalamic reticular nucleus generates thalamic bursts and cortical spindles. *Nature Neuroscience*, 14(9), 1118–1120. <https://doi.org/10.1038/nn.2880>
- Herrera, C. G., Cadavieco, M. C., Jego, S., Ponomarenko, A., Korotkova, T., & Adamantidis, A. (2016). Hypothalamic feedforward inhibition of thalamocortical network controls arousal and consciousness. *Nature Neuroscience*, 19(2), 290–298. <https://doi.org/10.1038/nn.4209>
- Hou, G., Smith, A. G., & Zhang, Z.-W. (2016). Lack of intrinsic GABAergic connections in the thalamic reticular nucleus of the mouse. *The Journal of Neuroscience*, 36(27), 7246–7252. <https://doi.org/10.1523/jneurosci.0607-16.2016>
- Kim, A., Latchoumane, C., Lee, S., Kim, G. B., Cheong, E., Augustine, G. J., & Shin, H. S. (2012). Optogenetically induced sleep spindle rhythms alter sleep architectures in mice. *Proceedings of the National Academy of Sciences of the United States of America*, 109(50), 20673–20678. <https://doi.org/10.1073/pnas.1217897109>
- Kim, D., Hwang, E., Lee, M., Sung, H., & Choi, J. H. (2015). Characterization of topographically specific sleep spindles in mice. *Sleep*, 38(1), 85–96. <https://doi.org/10.5665/sleep.4330>
- Kolmac, C. I., & Mitrofanis, J. (1998). Patterns of brainstem projection to the thalamic reticular nucleus. *Journal of Comparative Neurology*, 396(4), 531–543. [https://doi.org/10.1002/\(SICI\)1096-9861\(19980713\)396:4<531:AID-CNE9>3.0.CO;2-2](https://doi.org/10.1002/(SICI)1096-9861(19980713)396:4<531:AID-CNE9>3.0.CO;2-2)
- Lewis, L. D., Voigts, J., Flores, F. J., Ian Schmitt, L., Wilson, M. A., Halassa, M. M., & Brown, E. N. (2015). Thalamic reticular nucleus induces fast and local modulation of arousal state. *eLife*, 4(5), 2015. <https://doi.org/10.7554/eLife.08760>
- Li, Y., Lopez-Huerta, V. G., Adiconis, X., Levandowski, K., Choi, S., Simmons, S. K., Arias-García, M. A., Guo, B., Yao, A. Y., Blosser, T. R., Wimmer, R. D., Aida, T., Atamian, A., Naik, T., Sun, X., Bi, D., Malhotra, D., Hession, C. C., Shema, R., ... Feng, G. (2020). Distinct subnetworks of the thalamic reticular nucleus. *Nature*, 583(7818), 819–824. <https://doi.org/10.1038/s41586-020-2504-5>
- Lüthi, A. (2014). Sleep spindles: Where they come from, what they do. In *Neuroscientist* (Vol. 20, Issue 3, pp. 243–256). SAGE Publications Inc. <https://doi.org/10.1177/1073858413500854>
- McAlonan, K., Cavanaugh, J., & Wurtz, R. H. (2006). Attentional modulation of thalamic reticular neurons. *Journal of Neuroscience*, 26(16), 4444–4450. <https://doi.org/10.1523/JNEUROSCI.5602-05.2006>
- Mcginty, D. J., & Serman, M. B. (1968). Sleep suppression after basal forebrain lesions in the cat. *Science*, 160(3833), 1253–1255. <https://doi.org/10.1126/science.160.3833.1253>
- Ni, K. M., Hou, X. J., Yang, C. H., Dong, P., Li, Y., Zhang, Y., Jiang, P., Berg, D. K., Duan, S., & Li, X. M. (2016). Selectively driving cholinergic fibers optically in the thalamic reticular nucleus promotes sleep. *eLife*, 5(FEBRUARY2016), e10382. <https://doi.org/10.7554/eLife.10382>
- Pinault, D. (2004). The thalamic reticular nucleus: Structure, function and concept. In *Brain research reviews* (Vol. 46, Issue 1, pp. 1–31). Brain Res Brain Res Rev. <https://doi.org/10.1016/j.brainresrev.2004.04.008>
- Práwdicz-Neminski, W. W. (1925). Zur Kenntnis der elektrischen und der Innervationsvorgänge in den funktionellen Elementen und Geweben des tierischen Organismus. Elektrocerebrogramm der Säugetiere. *Pflügers Archiv für Die Gesamte Physiologie Des Menschen Und der Tiere*, 209(1), 362–382. <https://doi.org/10.1007/BF01730925>
- Schönauer, M., & Pöhlchen, D. (2018). Sleep spindles. In *Current biology* (Vol. 28, Issue 19, pp. R1129– R1130). Cell Press. <https://doi.org/10.1016/j.cub.2018.07.035>
- Shosaku, A., Kayama, Y., Sumitomo, I., Sugitani, M., & Iwama, K. (1989). Analysis of recurrent inhibitory circuit in rat thalamus: Neurophysiology of the thalamic reticular nucleus. In *Progress in neurobiology* (Vol. 32, Issue 2, pp. 77–102). Pergamon. [https://doi.org/10.1016/0301-0082\(89\)90011-7](https://doi.org/10.1016/0301-0082(89)90011-7)
- Siclari, F., & Tononi, G. (2017). Local aspects of sleep and wakefulness. In *Current opinion in neurobiology* (Vol. 44) (pp. 222–227). Elsevier Ltd. <https://doi.org/10.1016/j.conb.2017.05.008>
- Steriade, M., McCormick, D. A., & Sejnowski, T. J. (1993). Thalamocortical oscillations in the sleeping and aroused brain. *Science*, 262(5134), 679–685. <https://doi.org/10.1126/science.8235588>
- Steuillet, P., Cabungcal, J. H., Bukhari, S. A., Ardelt, M. I., Pantazopoulos, H., Hamati, F., Salt, T. E., Cuenod, M.,

- Do, K. Q., & Berretta, S. (2018). The thalamic reticular nucleus in schizophrenia and bipolar disorder: Role of parvalbumin-expressing neuron networks and oxidative stress. *Molecular Psychiatry*, 23(10), 2057–2065. <https://doi.org/10.1038/mp.2017.230>
- von Economo, C. (1930). Some new methods of studying the brain of exceptional persons (encephalometry and brain casts). *The Journal of Nervous and Mental Disease*, 71(3), 300–302. <https://doi.org/10.1097/00005053-193003000-00007>
- Vyazovskiy, V. V., Achermann, P., Borbély, A. A., & Tobler, I. (2004). The dynamics of spindles and EEG slow-wave activity in NREM sleep in mice. *Archives Italiennes de Biologie*, 142(4), 511–523. <https://doi.org/10.4449/aib.v142i4.422>
- Wells, M. F., Wimmer, R. D., Schmitt, L. I., Feng, G., & Halassa, M. M. (2016). Thalamic reticular impairment underlies attention deficit in Ptchd1 Y<sup>0</sup> mice. *Nature*, 532(7597), 58–63. <https://doi.org/10.1038/nature17427>
- Wimmer, R. D., Astori, S., Bond, C. T., Rovó, Z., Chatton, J. Y., Adelman, J. P., Franken, P., & Lüthi, A. (2012). Sustaining sleep spindles through enhanced SK2-channel activity consolidates sleep and elevates arousal threshold. *Journal of Neuroscience*, 32(40), 13917–13928. <https://doi.org/10.1523/JNEUROSCI.2313-12.2012>
- Winsky-Sommerer, R., Knapman, A., Fedele, D. E., Schofield, C. M., Vyazovskiy, V. V., Rudolph, U., Huguenard, J. R., Fritschy, J. M., & Tobler, I. (2008). Normal sleep homeostasis and lack of epilepsy phenotype in GABAA receptor  $\alpha 3$  subunit-knockout mice. *Neuroscience*, 154(2), 595–605. <https://doi.org/10.1016/j.neuroscience.2008.03.081>
- Zhang, F., Wang, L. P., Brauner, M., Liewald, J. F., Kay, K., Watzke, N., Wood, P. G., Bamberg, E., Nagel, G., Gottschalk, A., & Deisseroth, K. (2007). Multimodal fast optical interrogation of neural circuitry. *Nature*, 446(7136), 633–639. <https://doi.org/10.1038/nature05744>

## SUPPORTING INFORMATION

Additional supporting information can be found online in the Supporting Information section at the end of this article.

**How to cite this article:** Visocky, V., Morris, B. J., Dunlop, J., Brandon, N., Sakata, S., & Pratt, J. A. (2023). Site-specific inhibition of the thalamic reticular nucleus induces distinct modulations in sleep architecture. *European Journal of Neuroscience*, 1–16. <https://doi.org/10.1111/ejn.15908>